HHS Public Access

Author manuscript

J Appl Polym Sci. Author manuscript; available in PMC 2018 December 03.

Published in final edited form as:

J Appl Polym Sci. 2013 May 5; 128(3): 1804–1814. doi:10.1002/APP.38335.

Temperature Responsive Hydrogel with Reactive Nanoparticles

Li Xiao, **Austin B. Isner**, **J. Zach Hilt**, and **Dibakar Bhattacharyya**

Department of Chemical and Materials Engineering, University of Kentucky, Lexington, Kentucky 40506-0046

Abstract

The application of temperature responsive hydrogels with ion-exchange domain for nanoscale catalytic reactions is an emerging and attractive area because of the combination of individual unique features: temperature responsive tunability by the polymer domain and the high catalytic reactivity of the nanomaterial. Here, we report the entrapment and/or direct synthesis of reactive Fe and Fe/Pd nanoparticles (about 40–70 nm) in a temperature responsive hydrogel network (*N*-isopropylacrylamide (NIPAAm), and NIPAAm—PAA). These nanoparticles are stabilized in the hydrogel network and the dechlorination (using trichloroethylene, TCE, as a model compound) reactivity in water is enhanced and controllable in the temperature range of 30–34°C involving polymer domain transitions at lower critical solution temperature (LCST) from hydrophilic to collapsed hydrophobic state. Water fraction modulation of the network and the enhancement of pollutant partitioning by the thermally responsive polymers play an important role in the catalytic activity.

Keywords

catalysts; copolymers; gels; nanoparticles; stimuli-sensitive polymers

INTRODUCTION

Hydrogels are hydrophilic polymer networks that can absorb a large amount of water but not dissolve in water.[1–3] Responsive hydrogels can undergo a swelling transition in response to environmental stimuli, such as the changes in temperature, light, pH, etc.[4–7] Because of this unique feature, responsive hydrogels have received extensive attention in the fields of drug delivery,[8] bioseparation,[9] sensors, and optical transduction of chemical signals.[9,10] For example, the drug release from responsive hydrogels can be remotely controlled by the local heating of magnetic nanoparticles.[11] The same concept has been transferred to the application in catalytic reaction, which is particularly attractive due to the unique tunable and responsive properties as well as the improvement of reactive properties.[8–10] Specifically, the swelling and deswelling of the hydrogel with temperature change can control the loading/unloading of reactants in the hydrogel network, which in turn changes the reactivity. Poly (*N*-isopropylacrylamide) (PNIPAAm) is one of the most common and widely studied temperature responsive hydrogels with hydrophobic and hydrophilic phase transition at a

Correspondence to: D. Bhattacharyya (db@engr.uky.edu).

lower critical solution temperature (LCST) about 32°C.[12–14] Below the LCST, NIPAAm is hydrophilic and swells in aqueous media, while it becomes hydrophobic and collapses above the LCST. Attracted by these particular responsive properties with the change of temperature, PNIPAAm has been received considerable attention and has been successfully employed as a support for the synthesis of metal nanoparticles and smart catalyst.[15,16] For example, Lu et al. proved the adjustable catalytic reactivity with response to temperature change for Ag nanoparticles imbedded in PNI-PAAm-b-PS core-shell systems.[17] This extended use of hydrogel from biomedical field[18,19] to environmental application by incorporating catalyst and responsive prosperity.

One can also utilize the hydrogels in environmental catalysis (such as, organic pollutant degradation from water) if appropriate catalytic domain and selective reactant partitioning can be created. The quality of water has been always an important and demanding issue in the exploitation of natural water resources and remediation of contamination in recent years.[20,21] Hydrogels has been reported to be used as is for fouling control in water treatment.[22,23] In particular in the field of catalysis, we use this hydrogel immobilized nanoparticles for detoxification of organic chlorinated compounds from aqueous streams. Chlorinated organics such as trichloroethylene (TCE) and polychlorinated biphenyls (PCBs) are the most concerned water pollutants due to their high toxicity, persistence and various sources of distribution in environment.[24,25] In recent years, the creation and development of nanosized materials as a promising way for toxic chlorinated organics degradation and water pollution treatment have been widely studied and investigated.[26–28] Nanoscale metallic particles with high surface area and high binding energy of core electrons can enhance the interaction of the surface sites between the reactants and products.[29,30] For more rapid and complete degradation, a second element such as Pd, Pt, Ni, Cu, and Ag was added as a hydrogenation catalyst.[27] Among these, Fe and/or Fe/Pd are the most efficient and commonly used system. However, Fe and/or Fe/Pd nanoparticles naturally tend to aggregate due to the magnetic properties, which may lead to the loss of dechlorination reactivity.[31,32] Thus, immobilization of nanoparticles has drawn great interest due to the increasing demand in controlling nanoparticle aggregation and reactivity. Specifically, stabilizers, ligands and membrane supports have been used to stabilize and immobilize nanoparticles.[33,34] A common problem in using these supports is the sacrifice of nanoparticle reactivity. Moreover, the surfactant coating may hinder the transportation of reactant to the surface of the nanoparticles, which may reduce the reaction rate. To overcome these problems and enhance the nanoparticles' performance, we proposed to use a temperature responsive P(NIPAAm-AA) hydrogel as a promising network support to immobilize metallic nanoparticles for toxic chlorinated organics degradation. Furthermore, for environmental catalytic applications, the synthesis of Fe and Fe/Pd NPs in temperature responsive hydrogels allows the control of the microenvironment near the active reaction sites to modulate the reactivity. Although immobilization of iron and platform for other catalyst, such as acrylic acid in membrane platform are extensively published, to our knowledge, the platform with both hydrophobic and PAA for *in situ* synthesis of nanoparticles, and tunability of hydrophobic and hydrophilic domain have not been published with Fe and Fe/Pd nanoparticles.

The main goals of present study are: (i) to synthesize temperature responsive P(NIPAAm-AA) hydrogel with ion exchange groups (—COOH) for metal ion capture and subsequent

conversion to nanostructured zero-valent metal in the matrix, (ii) to characterize the swelling and partitioning of hydrogel and hydrogel nanocomposites to test the hypothesis that the use of temperature responsive hydrogels will allow the modulation of reduction reaction reactivity of toxic chlorinated organics with TCE as a model compound by altering pollutant partitioning and water content around reactive nanoparticles, (iii) to evaluate the tunable reactivity of a model toxic organic, TCE, dechlorination reaction by these temperature responsive immobilized nanoparticles.

MATERIALS

All chemicals were used as reagent grade. *N*-isopropylacrylamide (NIPAAm), acrylic acid (AA), poly (ethylene glycol) 600 dimethacrylate (PEG600DMA), 4-(4-dimethylaminophenylazo) aniline (DMPA), ethanol (>99.5%), ferrous chloride tetrahydrate ($FeCl_2 \cdot 4H_2O$), sodium borohydride ($NaBH_4$), sodium carboxymethyl cellulose (CMC, mean M_w = 90,000), trichloroethylene (TCE) were purchased from Sigma–Aldrich. Deionized ultrafiltered water (DIUF) was purchased from Fisher Scientific.

Synthesis of Crosslinked P(NIPAAm-AA) Hydrogel

The P(NIPAAm-AA) hydrogel was prepared by ultraviolet (UV) initiated free radical photopolymerization method, using reported methods,[6,7,11] and acrylic acid (AA) was also added to introduce the —COOH groups for metal ion pick up. Typically, three grams of NIPAAm, 1 g AA, 0.207 g PEG600DMA (molar ratio of NIPAAm : AA : PEG600DMA = 80 : 10 : 10), and 43 mg DMPA as initiator were added in a 20 mL vial; an equal weight amount of ethanol was added and then mixed together to get a uniform solution. The mixture was pipetted into two 15 × 15 cm^2 clamped glass plates with Teflon spacer to make the thickness to be 0.5 mm. The schematic of P(NIPAAm-AA) synthesis is shown in Figure 1. The glass plate was then transferred to a UV source (LESCO) at wavelength of 365 nm with 14.8 mW cm^{-2} intensity. UV photopolymerization was conducted for 5 min. Both sides of the hydrogel were exposed to UV source for every 30 s to make sure the same intensity during the polymerization. The hydrogel was carefully removed from the plates, placed in deionized water, and washed daily.

Preparation of P(NIPAAm-AA) Hydrogel Immobilized Fe Nanoparticles

Prior to Fe^{2+} ion exchange, P(NIPAAm-AA) hydrogels were immersed in NaCl (5–10 wt %) solution at pH 10 overnight to convert the —COOH to —COONa. In the next step, the hydrogel was washed with DIUF until the pH of the effluent became neutral. Then, the hydrogel was immersed in 200 mL 200 mg L^{-1} $FeCl_2$ solution at a pH of 5.5 for 4 h. Nitrogen gas was bubbled to minimize the oxidation of Fe^{2+}. The reduction with sodium borohydride (100 mL, 19 g L^{-1}) ensured the Fe^0 nanoparticle formation. The hydrogel immobilized nanoparticles were also stored in ethanol for future use in the reductive TCE degradation. The schematic of Fe^0 nanoparticles synthesized directly in the hydrogel network is shown in Figure 2.

Traditionally, the nanoparticles or metal can be incorporated by encapsulation during the polymer synthesis. Thus, for comparison, P(NIPAAm-AA) hydrogel encapsulated Fe

nanoparticles was also prepared. The desired amount of Fe^0 nanoparticles stabilized with 1wt% sodium carboxymethyl cellulose carboxylic (CMC) was mixed with the monomer solution and bath sonicated for 5 min. The UV polymerization was initiated by the addition of photo-initiator with the same polymerization procedure as described above. The Fe nanoparticles in solution phase with 1% CMC were prepared by using the reported methods.[35,36]

Swelling Study of P(NIPAAm-AA) Hydrogel and Hydrogel Nanocomposites at Different Temperatures

The swelling studies were carried out for pure hydrogel discs and hydrogel nanocomposite with 1 wt % loaded nanoparticles in the temperature range of 15–45°C. The dry hydrogel weight was measured before placing in water baths maintained at set temperatures. The samples were taken out periodically, wiped with tissue to remove surface water and weighed until the swelling equilibrium was achieved. For each system, three samples were used to get averaged swelling ratios. The swelling ratio (Q) was calculated for each sample by[11] $Q = W_S/W_O$, where W_S is the weight of swollen sample, and W_O is the weight of dry samples.

Hydrophobicity and Hydrophilicity Transitions of Temperature-Responsive Hydrogel by Model Organic Partitioning Experiments

The hydrogel hydrophobicity and hydrophilicity was investigated by two different dyes: methylene blue and orange II. About 0.01 mmol L^{-1} methylene blue and orange II solution was prepared in advance. The hydrogels were immersed into 20 mL of the two solutions respectively at different temperatures for 24 h. The concentrations in solution phase before and after the immersion were measured by UV–vis spectroscopy with the reading of wavelength at 664 nm for methylene blue and 486 nm for orange II.[37,38] The partitioning coefficients (K) at different temperatures were calculated based on the initial and final concentrations of these two dyes. The partition coefficient (K) was defined as the ratio of the dye solubility in hydrogel and solubility in water.

The Reduction of TCE with P(NIPAAm-AA) Hydrogel Immobilized Nanoparticles

Batch dechlorination experiments of TCE were conducted in 43-mL serum glass vials. Fe or Fe/Pd NPs immobilized in a P(NIPAAm-AA) hydrogel were loaded into the vial containing 30 mg L^{-1} TCE in 43 mL deoxygenated water. The experiment was also carried out at 30 and 34°C to investigate the reactivity tunability. All the serum glass vials were sealed with Teflon-lined silicon septa and placed on a wrist-action shaker throughout the duration of the experiment. Parallel control experiments with only hydrogel (no metal nanoparticles) were also performed. TCE analysis was performed using a gas chromatograph (GC, Varian-3900) equipped with an ion-trap mass spectrometer (MS, Saturn-2100T). Two milliliter of pentane as the extractant for TCE was added to an 8-mL vial containing 2 mL of aqueous solution which was taken from the reaction vial. The vials were placed on the shaker to mix for 2 h to achieve extraction equilibrium. For each extracting vial, 1-μL solution in the extracting solvent phase was removed and injected into the GC sample column for analysis. The 1,2-dibromoethene was used as an internal standard. External standards of TCE were used to prepare calibration curves. The calibration curves were linear over the concentration range of 5–50 mg L^{-1} ($R^2 > 0.999$, regressions were based on the five-point calibration).

Chloride Analysis

The concentration of chloride ion as the main product of TCE degradation in aqueous solution was measured by the Orion 94-17 Solid State half-cell and Orion 96-17 iron plus Sure-Flow with Chloride Electrode. In all cases, the instrument calibration was based on commercial standards (Fisher Scientific) containing 1000 mg L^{-1} of the chloride with R^2 = 0.994 and an average analytical error of 3%. Nearly 2% (volume) of sodium nitrate (LabChem, 5 mol L^{-1}) was added into the samples as the ionic strength adjuster (ISA) to ensure the same ionic strength.

Metal Analysis

The amount of Fe captured during ion exchange and the amount of Pd in the hydrogel were quantified by using a Varian SpectrAA 220 Fast Sequential atomic absorption spectrometer equipped with a Fisher Scientific hollow cathode lamp. For Fe, the lamp was operated at a wavelength of 386.0 nm. The calibration plot was created using four different concentrations of Fe ranging from 25 to 200 mg L^{-1} with R^2 = 0.9998 and an average analytical error of 2%. In the case of Pd, the lamp was operated at a wavelength of 246.6 nm and the linear calibration range was between 0.2 and 28 mg L^{-1} Pd. The error of analysis was <2% with R^2 = 0.9996.

Characterization of Hydrogel and Hydrogel Immobilized Nanoparticles

Surface and cross-section of hydrogel and hydrogel nanocomposites were examined by Hitachi S-4300 scanning electron microscope (SEM). Hydrogels were coated with gold for imaging purposes. To observe the real structure of hydrogel, the swollen gel was quickly frozen in liquid nitrogen and freeze dried for 48 h to get rid of water. Attenuated total reflectance Fourier transform infrared (ATR-FTIR) (Varian 7000e) was used to determine the presence of functional groups in hydrogel. The samples were placed on the diamond crystal and the spectrum was obtained between 500 and 4000 cm^{-1} for 32 scans at a resolution of 8 cm^{-1}.

RESULTS AND DISCUSSION

Synthesis of P(NIPAAm-AA) Hydrogel

The synthesis of both free radical redox and photopolymerization of NIPAAm hydrogel with PAA has extensively reported in the literatures.[39–41] These types of polymers have been extended further to layer-by-layer assembly on the surface.[42] On the other hand, our work is to create hydrogel along with ionizable groups such as: carboxylic groups to sorb metal ions for postreduction with reduce agent to form nanoparticles for catalysis. This brings in catalytic aspects domain which is an important area particularly environmental area. This section addresses specific aspects of the UV based polymerization steps.

Important variables in the polymerization and morphology change are AA and NIPAAm ratios, and thus the hydrogel including charge groups with different morphologies can be created. The synthesis flowchart for the P(NIPAAm-AA) hydrogel and the corresponding mechanism are shown in Figure 1. It should be pointed out that the thickness of hydrogel can be easily changed by adjusting the spacer thickness. The first stage was to characterize

the polymerization steps by using ATR-FTIR. From the ATR-FTIR spectra as shown in Figure 3, the peak at 1700 cm^{-1} is assigned to the C = O group in AA, and the peak at 1650 cm^{-1} belongs to the overlapping of NIPAAm and AA ranging from 1610 to 1660 cm^{-1}. The band at 1550 cm^{-1} is assigned to the N—H vibration of NIPAAm.[12] The appearance of these peaks in the P(NIPAAm-AA) hydrogel demonstrates the successful copolymerization of NIPAAm and AA.

Figure 4(A, B) show the SEM image of P(NIPAAm-AA) surface and cross-sectional structure. Clearly, the hydrogel shows a porous structure which is beneficial for the increase of accessibility toward the immobilized metallic nanoparticles. In this article, AA was utilized to pick up iron ions and therefore immobilize metallic nanoparticles into the hydrogel network. The thermosensitive NIPAAm segments can swell and deswell reversibly, which can in turn adjust the concentration of toxic organics and the immobilized nanoparticles in the hydrogel matrix that can modify the reduction reaction.[17] Furthermore, the swelling/deswelling facilitates the regeneration and the reusability of nanoparticles.

Synthesis of Reactive Fe Nanoparticles in P(NIPAAm-AA) Hydrogel

As reported, the metal ion can also be bonded to the nitrogen atom from amide group in NIPAAm chain but with lower affinity to ferrous ions.[43] Thus, in our work, free —COOH groups from PAA segment in the hydrogel was utilized to sorb metal ions for postreduction by reducing agent. It has been reported that one ferrous ion can be complexed with two —COOH groups.[44] The mass balance of ferrous ions was calculated based on the atomic adsorption (AA) analysis of the $FeCl_2$ solution before and after the loading of Fe^{2+} in the hydrogel. Assuming all the acrylic acid was polymerized in the final copolymer, so the amount of acrylic acid should be 0.9 mmol for per gram of dry hydrogel weight. Base on this number, assuming all carboxylic groups are ionized and can be complexed with Fe^{2+}, the ration of Fe^{2+} to —COOH should be 0.5. On the basis of the results from AA analysis, our experimental value is 0.6, which is quite reasonable. The bounded metal ions were reduced with $NaBH_4$ to form Fe nanoparticles. Correspondingly, the color of hydrogel changes from white to black due to the formation of Fe^0 nanoparticles inside the hydrogel network as shown in the corresponding digital photos in Figure 2. Because the reduction of Fe with borohydride has been well studied and established, the total iron (Fe^0) was also analyzed. According to the AA analysis results and mass balance, a 94% yield of Fe nanoparticles was achieved after the reduction of bound Fe^{2+} with $NaBH_4$. This value agrees well with the established PAA metal binding stability constant.

It is worth noting that the formed Fe nanoparticles often have a very thin oxide layer on the surface even for the freshly made and nitrogen protected nanoparticles. Literatures[45,46] have demonstrated the formed nanoparticles always contain a core-shell structure with Fe nanoparticles as core and oxide as shell by spectroscopy and electrochemistry, but these nanoparticles are still very reactive and can be used for toxic organics degradation according to the results of the reductive reaction study. Actually, these oxide shells impart some stability to these Fe nanoparticles in solution phase, because the nanoparticles are very easy to aggregate in solution to form cluster leading to the decrease of reactivity. This is also the

reason for using various stabilizers, and one of the advantages of the use of hydrogel network in this work is to prevent the oxidation and aggregation of the nanoparticles.

For better comparison, Fe^0 nanoparticles immobilized in hydrogel by encapsulation of preformed nanoparticles were also prepared. As shown in the SEM images, Fe^0 nanoparticles directly synthesized in the hydrogel [Figure 5(A)] are roughly spherical with a homogeneous distribution and an average size of about 40 nm which was smaller than those encapsulated in a hydrogel network (100 nm) [Figure 5(B)]. By using this method with PAA metal ion binding followed by reduction, iron nanoparticles can be created with uniform distribution inside the matrix, which can prevent the migration and nanoparticles aggregation. This is important in stabilizing the nanoparticles and controls the size of particles.[47]

Swelling Study of Temperature Responsive P(NIPAAm-AA) Hydrogel

Swelling/shrinking in water by temperature change is a unique feature of hydrogel, and has been widely studied by many researchers.[48,49] The driving force of swelling/shrinking below and above volume phase transition temperature is usually considered to be the formation of hydrogen bonds with water and the hydrophilicity and hydrophobicity transition which is controlled by the property changes of side chain of NIPAAm.[12–14] This work takes the advantages of swelling/shrinking feature of hydrogel to manipulate the reduction of toxic organics by controlling the water content in the hydrogel network.

Water plays an important role in the toxic organics reduction by Fe because it can facilitate the corrosion of the Fe to provide hydrogen and electrons which can be utilized to replace chlorine in the reduction of toxic chlorinated organics.[44] But too much water may oxidize the nanoparticles and decrease the reactivity. So by utilizing the swelling/shrinking feature of temperature responsive hydrogel, water content in the hydrogel network can be modulate, which in turn can tune the toxic chlorinated organics reduction reaction.

The preliminary swelling ratio of the hydrogel at different temperatures was investigated to study the water content in the hydrogel matrix as shown in Figure 6. The swelling ratio decreases with the increasing of temperature. The observed water content decrease in hydrogel at higher temperatures is consistent with the phase change behavior. In addition, the presence of nanoparticles in the nanocomposite hydrogel does not appear to have significant effects on the swelling ratio, which may be because of the free space left after the *in situ* reduction of nanoparticles.[15] For complete degradation of TCE ($C_2HCl_3 + 4Fe^0 + 5H_2O \rightarrow C_2H_6 + 4Fe^{2+} + 3Cl^- + 5OH^-$),[35] the minimum water amount for completely TCE dechlorination (30 mg L^{-1}, 40 mL) was calculated to be only 0.8 mg, and the excess water may cause the iron corrosion ($Fe^0 + 2H_2O \rightarrow Fe^{2+} + H_2 + 2OH^-$) and less reactivity. Therefore, by utilizing the temperature responsive hydrogel, the water content can be properly adjusted and modulate the reaction.

Establishment of Hydrophobicity and Hydrophilicity Transitions of Temperature Responsive Hydrogel by Model Organic Partitioning Experiments

For catalytic important material, molecule transport in hydrogel is important and only can occur in the confined space within the polymer chain.[50,51] And thus, any factors that can

reduce this space size, like hydrophobicity and hydrophilicity transition, would also affect the transportation of molecule through hydrogel network. Thus it is important to establish quantitatively the role of hydrophobicity and hydrophilicity of hydrogel. For such purpose, partition coefficient (K) defined as the ratio of solubility in hydrogel and in water phase, was determined through the use of two model compounds: methylene blue and orange II.[37,38] These two compounds have similar molecular weight, which can minimize the effects of the molecular size on the affinity with the hydrogel. The comparison of the two structures indicates that orange II is more hydrophilic than methylene blue due to the facile formation of hydrogen bonds in the orange II molecule.[37,38] The raise of solubility of methylene blue in swollen hydrogel was observed when the hydrogels were heated from 10 to 45°C [Figure 7(A)], while the orange II shows opposite solubility change behavior [Figure 7(B)]. Such observation is consistent with the phase change of temperature responsive segment NIPAAm. When the temperature increases, the existence of NIPAAm makes the network to change from hydrophilic to hydrophobic, during which the diffusion of orange II is reduced by the non-polar groups and in turn, and the solubility decreases.

Reductive Reaction by Hydrogel Immobilized Nanoparticles

The model compound utilized for reductive reaction is a well-known pollutant in ground water, trichloroethylene (TCE), and the objective of this reductive transformation is to convert Cl to H, which is commonly referred by environmental literature as dechlorination. It is well known that the reductive reaction by Fe nanoparticles is through electron transfer mechanism which are generated from Fe^0 corrosion; while in the Fe/Pd bimetallic system, H_2 was generated by Fe corrosion and Pd acts as a catalyst (the dechlorination occurs on Pd surface).[32,52,53] The reductive degradation of chlorinated organics with zero valent metallic nanoparticles is a heterogeneous reaction, which include the adsorption of TCE on the particles surface, surface of reaction and desorption.[44] As a reactant, TCE concentration can affect the reductive reaction. Our previous work has established a mathematical model to study the transport of the reactant (such as TCE) to the reactive sites by adsorption and demonstrated that the surface TCE saturation has insignificant effect on the reaction mechanistic pathways.[29] The Langmurian-type quasisorption isotherm model in this literature was utilized to study the TCE adsorption and the effects of TCE concentration on the degradation reaction. The result showed at the higher TCE concentration (500 mg L^{-1}), the total surface of nanoparticles (2.5 g L^{-1}) covered by TCE molecules has reached a saturation, and there is no more available sites for TCE adsorption. However, in our work, dilute TCE feed concentration (30 mg L^{-1}) was used for environmental application and the iron loading concentration is considerably higher than the theoretical requirement. So the complete degradation of TCE would be expected.

The dechlorination performance for Fe^0 nanoparticles immobilized in a hydrogel network is shown in Figure 8. Most of the bound chloride was converted to Cl^-. Some points were taken in duplicate, which shows a good reproducibility and stability (no nanoparticle deactivation observed). The reductive degradation rate in batch system can be described by the pseudo-first-order model[30]: $dC/dt = k_{obs}C = k_{SA}a_S\rho_m C$, where "$a_S$" is the specific surface area of the nanoparticles (m^2 g^{-1}) and ρ_m is the nanoparticle loading (g L^{-1}). Figure 8 is the normalized reactivity per unit metal surface area to get better comparison of the

reaction rates at different operating conditions. Logarithmic values of TCE concentrations are plotted versus time and best linear fit values of the k_{SA} can be obtained by using the experimental degradation results. Assuming discreet spherical particles with a diameter of 40 nm, as observed from SEM image, a_S was calculated to be 20 m^2 g^{-1} Based on these assumptions, the calculated k_{SA} values for the nanoparticles for DIUF water dechlorination were determined to be 0.0066 L m^{-2} h^{-1} for *in situ* synthesized Fe^0 in P(NIPAAm-AA) hydrogel and 0.0036 L m^{-2} h^{-1} for Fe^0 encapsulated in hydrogel as shown in Figure 9. In this case, the concentration of chloride, the only product of reduction reaction was also measured to determine the reactivity. In case of complete TCE degradation, 1 mole of TCE degraded can yield 3 moles of chloride. The chloride balances were defined as the ratio of detected chloride ($[Cl^{-1}]$) over the theoretical formation of chloride ($[Cl^{-1}]_{max}$) calculated from the TCE degradation data. The formed chloride balances obtained in the above systems were about 90%. The chloride loss can be explained by the sorption of chloride ions on to hydrogels and nanoparticles.[44,53] Beside the deactivation by iron hydroxide formed on the metal surface without hydrogel matrix, the reaction rates difference is probably due to the small and uniform particles directly formed in the matrix. Nanoparticles without any polymer support may cause excessive aggregation of metal atoms. Because TCE degradation rates highly depend on the total surface area of metal particles,[33] the excessive aggregation of particles in solution phase and in hydrogel phase by external encapsulation may cause less surface area or loss of the available reactive sites which results in the decrease of k_{SA}. Also, the more free spaces left after direct reduction within the networks may facilitate the transportation of TCE inside the hydrogel network and as well as enhance the reaction on the reactive sites of the nanoparticles.[30] It is also important to mention that during TCE degradation, the Fe^{2+}/Fe^{3+} ions that are formed from the reactant Fe^0 are recaptured by the carboxylic acid groups from acrylic acid. This not only can prevent the formation of precipitate that can inhibit the dechlorination reaction, but also make it easy for recovered ions to be regenerated to the metal form.[34] In contrast to the homogeneous phase nanoparticles applications, our approach has negligible loss of iron to solution phase.

In addition, TCE degradation was also conducted with sample water from a contaminated site in Paducah, KY containing 82 mg L^{-1} alkalinity, 293 mg L^{-1} total dissolved solids and 1.2 mg L^{-1} turbidity. The detailed water quality analysis was reported in literature.[54] As shown in Figure 8, the difference of degradation results between DIUF and sample water was within 2% for the same feed TCE concentration, which indicates the insignificant impact of hydrogel network on dechlorination in the contaminated sites. This also demonstrates that our system can be applied to the real world. It should be noticed that control experiments were also conducted to prove that TCE evaporation and physical adsorption in hydrogel has no effects on the TCE degradation. The whole hydrogel was extracted with pentane and no TCE detected by GC-MS and also, the TCE concentration was within 10% of the original value, which can prove that TCE concentration decrease during dechlorination studies is completely due to reaction with Fe nanoparticles.

Role of Temperature Responsive Behavior

There are extensive literatures on the role of temperature on the catalytic behavior of Fe and Fe/Pd on various degradation reactions.[55–57] On the other hand, the simultaneous role of

hydrophilic and hydrophobic domain in temperature domain in hydrogel along with reactivity is a new area. The reaction rate discussed here is the overall reaction rate including the intrinsic reaction rate and adsorption rate of TCE to reactive sites of nanoparticles.[29,34]

TCE adsorption on reactive sites can be achieved by transfer in aqueous phase or diffusion in hydrogel matrix.[44] TCE diffusion rate in hydrogel matrix is higher than the rate in aqueous phase because of the enhancement of hydrophobicity at higher temperature above LCST.[12–14] When the temperature increases, the hydrogel become hydrophobic and thus lead to a strong interaction with hydrophobic compounds such as TCE, i.e., a higher partitioning rate for TCE. Based on the TCE adsorption experiment for 24 h as shown in Figure 9, only 30% of TCE was adsorbed at 23°C (below LCST), while it was increased to 65% at 34°C (above LCST). However, the TCE adsorption through PAA hydrogel shows degrease of adsorption amount when temperature increases, which shows the importance of hydrophobic property of NIPAAm segment. Therefore, in addition to the prevention of agglomeration of nanoparticles, another advantage of using the temperature responsive hydrogels is the potential change in observed particle reactivity via the temperature change in state.

To demonstrate the effects of temperature on the reduction reactivity with hydrogel nanocomposites, the dechlorination performance by Fe/Pd bimetallic nanoparticles immobilized in a hydrogel were studied at 34 and 30°C, which cover the polymer domain transitions from hydrophilic to collapsed hydrophobic state as shown in Figure 10. The surface area normalized reaction rate (k_{SA}) for Fe/Pd (1.5 wt % as of Fe) immobilized in P(NIPAAm-AA) hydrogel indicated three times increase from 0.0156 to 0.0411 L m^{-2} h^{-1}. For comparison, dechlorination with Fe/Pd in solution phase was also conducted and showed only two times increase of reactivity, which demonstrates the primary role of partitioning increase in the reactivity improvement via temperature change for hydrogel immobilized nanoparticle. It should be mentioned that the reactivity here is lower than the referenced value.[51] That may be due to the reason that Fe/Pd reactivity is a strong function of Pd loading amount, and the TCE dechlorination rates could vary by one to five orders of magnitude by changing the Pd loading amount.[29,32] The TCE diffusion rate in hydrogel networks should be faster than that in the aqueous phase when the hydrophobicity of the hydrogel increases via a temperature increase, helping to enhance the overall dechlorination rate as shown in Figure 11. In addition, the calculated nanoparticles volume fraction was increased by more than two times, which can expectedly lead to the enhancement of dechlorination reactivity. The discussion may lead to the question why not use hydrophobic polymer immobilized catalyst and do the reaction and the same result could be obtained. Part of this statement is true, but truly hydrophobic polymer cannot make hydrogels with porous network and the synthesis of nanoparticles in this domain without any water is also not possible. On the other hand, the hydrophilic and hydrophobic copolymer used in this work can perfectly fit the needs.

Our lab has reported the PAA functionalization of membrane with subsequent Fe and Fe/Pd nanoparticles immobilization to degrade a variety of toxic chlorinated organic compounds.[58,59] Here, P(NIPAAm-AA) hydrogel was utilized because of the demand of not only transition but also hydrophilic ion exchange sites, like —COOH. The use of PAA hydrogel without NIPAAm could make it difficult to modulate hydrophobicity in the same platform.

In addition, some minimum water content is required to maintain the reaction as the reactivity will drop to zero[44] if iron nanoparticles are placed in completely hydrophobic domain such as polydimethylsiloxane (PDMS). Therefore, by the use of P(NIPAAm-AA) hydrogel, all of these requirements about balanced hydrophobicity and hydrophilicity, minimum water content and ion exchange groups, post capture of dissolve Fe can be achieved. Here, it should be pointed out that the cycle for TCE degradation between low temperature (below LCST) and high temperature (above LCST) was just used to prove the concept that the use of temperature responsive hydrogel can modulate the dechlorination reaction reactivity by control the water content in the matrix and enhance the affinity and partitioning of hydrophobic TCE to the polymer matrix. Even though the high temperature above LCST of NIPAAm is impractical in real water treatment application, the main purpose is to look at the fundamental aspects. Furthermore, the transition temperature can be decreased by introduction of hydrophobic moiety into the copolymer as widely reported in the literatures.[60–62]

A common problem for using nanoparticles in solution phase is that the oxidation of iron by dissolved O_2 in water and iron corrosion by water can lead to the loss of iron and formation of precipitates. In contrast, the use of hydrogel with the carboxylic groups can effectively prevent precipitation to give longevity. Our preliminary study with a multitrial TCE dechlorination studies (6 h for one trial) proved no loss of reactivity even after 3 days' storage, which can be very practical for environmental application to prevent aggregation and loss of reactivity as compared to conventional nanoparticles.

CONCLUSIONS

In conclusion, temperature responsive P(NIPAAm-AA) hydrogel prepared by free radical polymerization have been investigated as templates for the *in situ* formation of nanosized Fe particles with uniform size and distribution. The hydrogel immobilized Fe nanoparticles showed a strong reactivity for the reductive degradation of a model toxic chlorinated organic, a common pollutant, TCE and could be recyclable and reused. Furthermore, the reduction reaction rate was modulated by taking advantage of hydrophobic and hydrophilic transitions (30–34°C) through controlling the swelling and collapse of the hydrogel at LCST of temperature responsive hydrogel. The development of reactive polymer hydrogel with nanoparticles and controlled partitioning should lead applications ranging from organic synthesis to pollution control.

ACKNOWLEDGMENTS

This research was supported by National Institute of Environmental Health Sciences Superfund Research Program (NIEHS-SRP) and by the US Department of Energy (DOE) KRCEE programs.

REFERENCES

1. Lai J; Fang R; Wang L-Q; Tu K; Zhao C; Qian X; Zhan SJ Appl. Polym. Sci. 2009, 113, 3944.
2. Yoshida M; Lahann J ACS Nano 2008, 2, 1101. [PubMed: 19206325]
3. Wang R; Hashimoto K; Fujishima A; Chikuni M; Kojima E; Kitamura A; Shimohigoshi M; Watanabe T Nature 1997, 388, 431.
4. Wang Q; Li S; Wang Z; Liu H; Li CJ Appl. Polym. Sci. 2009, 111, 1417.

5. Estillore NC; Advincula RC Langmuir 2011, 27, 5997. [PubMed: 21513321]
6. Peppas NA; Hilt JZ; Khademhosseini A; Langer R Adv. Mater. 2006, 18, 1345.
7. Satarkar NS; Biswal D; Hilt JZ Soft Matter 2010, 6, 2364.
8. Stuart MAC; Huck WTS; Genzer J; Muller M; Ober C; Stamm M; Sukhorukov GB; Szleifer I; Tsukruk VV; Urban M; Winnik F; Zauscher S; Luzinov I; Minko S Nat. Mater. 2010, 9, 101. [PubMed: 20094081]
9. Tokarev I; Minko S Soft Matter 2009, 5, 511.
10. Wandera D; Wickramasinghe SR; Husson SM J. Membr. Sci. 2010, 357, 6.
11. Satarkar NS; Hilt JZ J. Controlled Release 2008, 130, 246.
12. Schild HG Prog. Polym. Sci. 1992, 17, 163.
13. Gorey C; Escobar IC J. Membr. Sci. 2011, 383, 272.
14. Du H; Wickramasinghe R; Qian XJ Phys. Chem. B 2010, 114, 16594.
15. Gan D; Lyon LA Macromolecules 2002, 35, 9634.
16. Bergbreiter DE; Case BL; Liu YS; Caraway JW Macromolecules 1998, 31, 6053.
17. Lu Y; Mei Y; Drechsler M; Ballauff M Angew. Chem. Int. Ed. 2006, 45, 813.
18. Neoh KG; Kang ET MRS Bull, 2010, 35, 673.
19. Whittell GR; Hager MD; Schubert US; Manners I Nat. Mater. 2011, 10, 176. [PubMed: 21336298]
20. Sahiner N; Ozay H; Ozay O; Aktas N Appl. Catal. A Gen. 2010, 385, 201.
21. Postel SL Science 2006, 313, 1046.
22. Wang JJ; Liu FJ Appl. Polym. Sci. 2012, 125, 548.
23. La Y-H; McCloskey BD; Sooriyakumaran R; Vora A; Freeman B; Nassar M; Hedrick J; Nelson A; Allen RJ Membr. Sci. 2011, 372, 285.
24. Doty SL; Shang TQ; Wilson AM; Tangen J; Westergreen AD; Newman LA; Strand SE; Gordon MP Proc. Natl. Acad. Sci. 2000, 97, 6287. [PubMed: 10841534]
25. Brown JF; Bedard DL; Brennan MJ; Carnahan JC; Feng H; Wagner RE Science 1987, 236, 709. [PubMed: 17748310]
26. Matheson LJ; Tratnyek PG Environ. Sci. Technol. 1994, 28, 2045. [PubMed: 22191743]
27. Clancy P Nat Nano 2011, 6, 540.
28. Pradeep T; Anshup S Thin Solid Films 2009, 517, 6441.
29. Tee YH; Bachas L; Bhattacharyya DJ Phys. Chem. C 2009, 113, 9454.
30. Wang CB; Zhang WX Environ. Sci. Technol. 1997, 31, 2154.
31. Shannon MA; Bohn PW; Elimelech M; Georgiadis JG; Marinas BJ; Mayes AM Nature 2008, 452, 301. [PubMed: 18354474]
32. Tratnyek PG; Johnson RL Nano Today 2006, 1, 44.
33. Phenrat T; Saleh N; Sirk K; Kim H-J; Tilton R; Lowry GJ Nanopart. Res. 2008, 10, 795.
34. Lewis SR; Datta S; Gui M; Coker EL; Huggins FE; Daunert S; Bachas L; Bhattacharyya D Proc. Natl. Acad. Sci. USA 2011, 108, 8577. [PubMed: 21606340]
35. He F; Zhao D Appl. Catal. B 2008, 84, 533.
36. He F; Zhao D Environ. Sci. Technol. 2007, 41, 6216. [PubMed: 17937305]
37. Guilherme MR; Silva R; Girotto EM; Rubira AF; Muniz EC Polymer 2003, 44, 4213.
38. Muniz EC; Geuskens GJ Membr. Sci. 2000, 172, 287.
39. Adem E; Burillo G; Bucio E; Magaña C; Avalos-Borja M Radiat. Phys. Chem. 2009, 78, 549.
40. Chen S; Jiang L; Dan YJ Appl. Polym. Sci. 2011, 121, 3322.
41. Liu S; Liu X; Li F; Fang Y; Wang Y; Yu JJ Appl. Polym. Sci. 2008, 109, 4036.
42. Díez-Pascual AM; Wong JE J. Colloid Interface Sci. 2010, 347, 79. [PubMed: 20385389]
43. Li W; Zhao H; Teasdale PR; John R; Zhang S React. Funct. Polym. 2002, 52, 31.
44. Xu J Synthesis and Reactivity of Membrane-supported Bimetallic Nanoparticles for PCB and Trichloroethylene Dechlorination; PhD. Thesis, University of Kentucky, Lexington, KY, 10 2007.
45. Nurmi JT; Tratnyek PG; Sarathy V; Baer DR; Amonette JE; Pecher K; Wang C; Linehan JC; Matson DW; Penn RL; Driessen MD Environ. Sci. Technol. 2004, 39, 1221.

46. Mulvaney P In Nanoscale Materials in Chemistry; Klabunde, K. J, Ed.; Wiley: New York, 2002; Chapter 5, p 121.
47. Ritchie SMC; Kissick KE; Bachas LG; Sikdar SK; Parikh C; Bhattacharyya D Environ. Sci. Technol. 2001, 35, 3252. [PubMed: 11506016]
48. Mohan YM; Murthy PSK; Sreeramulu J; Raju KM J. Appl. Polym. Sci. 2005, 98, 302.
49. Yu H; Grainger DW J. Appl. Polym. Sci. 1993, 49, 1553.
50. Ghosh RJ Membr. Sci. 2001, 192, 145.
51. Kiso Y; Sugiura Y; Kitao TJ Membr. Sci. 2001, 192, 1.
52. Lien HL; Zhang WX Colloids Surf. Physicochem. Eng. Aspects 2001, 191, 97.
53. Xu J; Dozier A; Bhattacharyya DJ Nanopart. Res. 2005, 7, 449.
54. Meyer DE; Hampson S; Ormsbee L; Bhattacharyya D Environ. Progr. Sustain. Energy 2009, 28, 507.
55. Bransfield SJ; Cwiertny DM; Livi K; Fairbrother DH Appl. Catal, B 2007, 76, 348.
56. Borgschulte A; Westerwaal RJ; Rector JH J. Catal. 2006, 239, 263.
57. Parshetti GK; Doong R-A Chemosphere 2012, 86, 392. [PubMed: 22115467]
58. Smuleac V; Varma R; Baruwati B; Sikdar S; Bhattacharyya D ChemSusChem 2011, 4, 1773. [PubMed: 22086852]
59. Smuleac V; Bachas L; Bhattacharyya DJ Membr. Sci. 2010, 346, 310.
60. Debord JD; Lyon LA Langmuir 2003, 19, 7662.
61. Feil H; Bae YH; Jan F; Kim SW Macromolecules 1993, 26, 2496.
62. Kuckling D; Harmon ME; Frank CW Macromolecules 2002, 35, 6377.

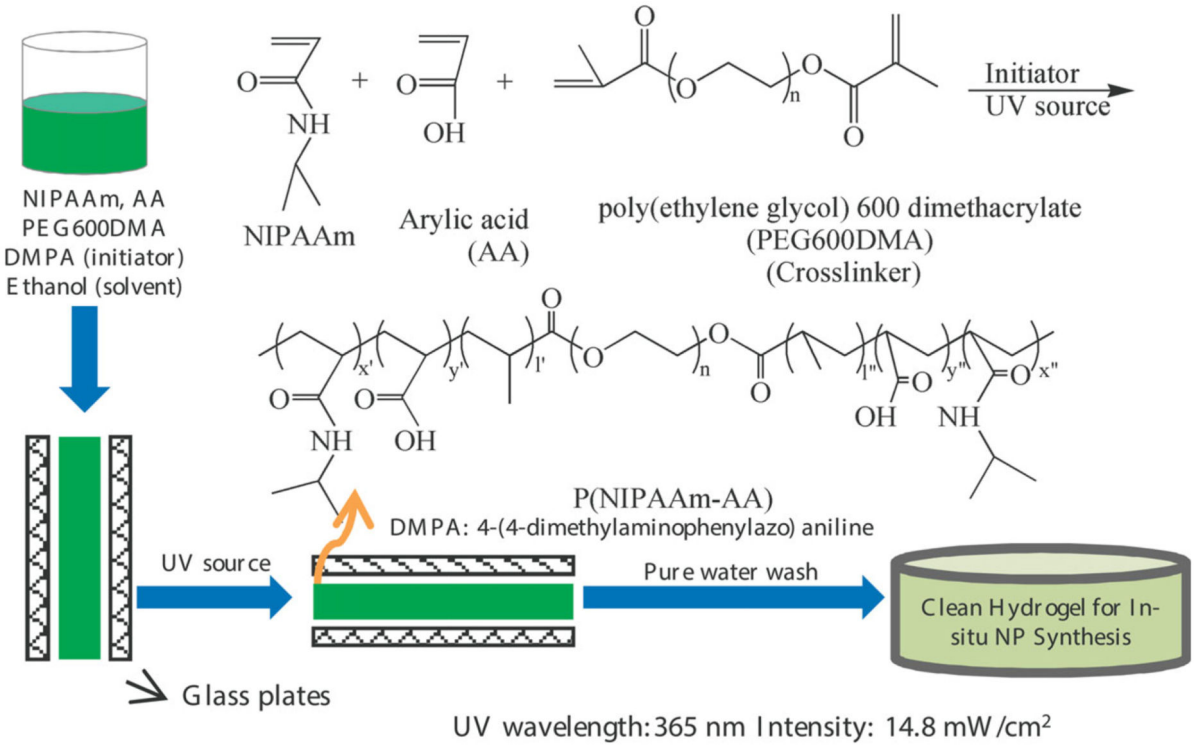

Figure 1.

Schematic diagram of P(NIPAAm-AA) by UV photopolymerization. [Color figure can be viewed in the online issue, which is available at wileyonlinelibrary.com.]

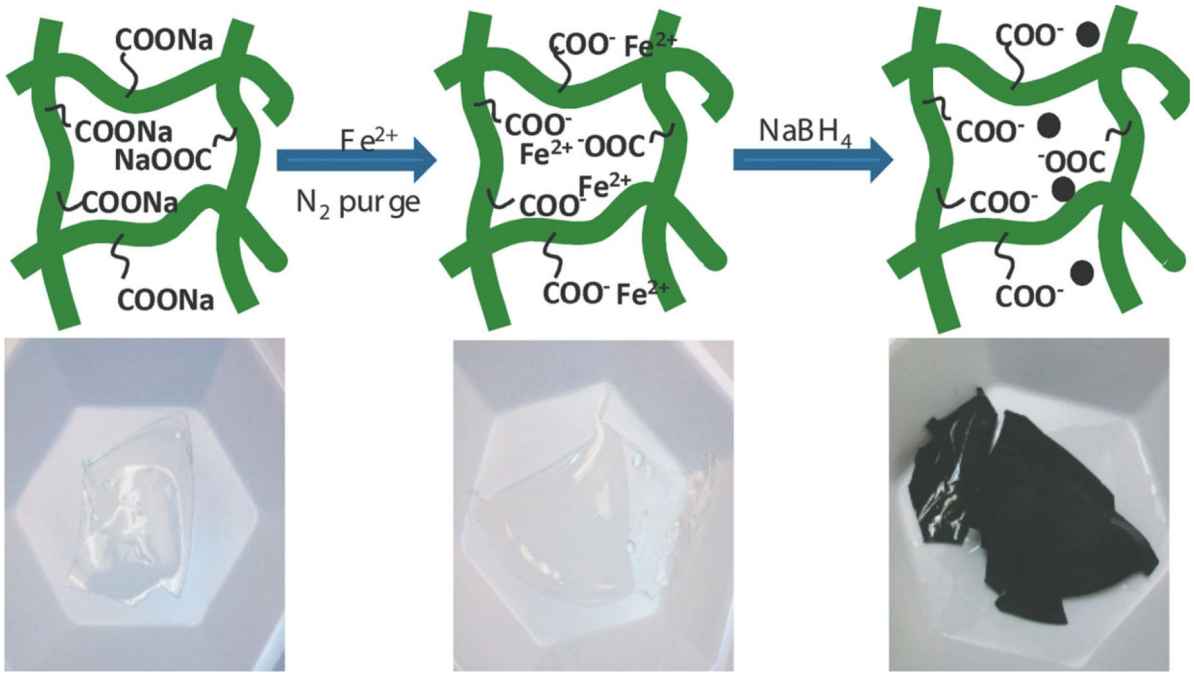

Figure 2.

Schematic of direct formation of Fe^0 nanoparticles in P(NIPAAm-AA) hydrogel network (upside) and the corresponding digital camera images (underside). [Color figure can be viewed in the online issue, which is available at wileyonlinelibrary.com.]

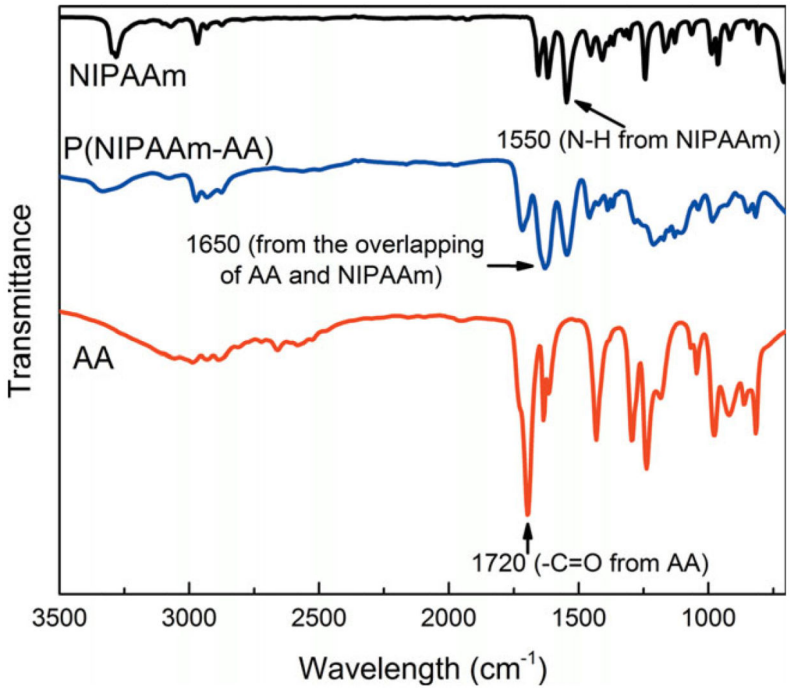

Figure 3.

ATR-FTIR spectra of P(NIPAAm-AA) hydrogel (green), NIPAAm (blue) and AA (red) monomers. The percentage of transmission scales varied in the range 100–30%. [Color figure can be viewed in the online issue, which is available at wileyonlinelibrary.com.]

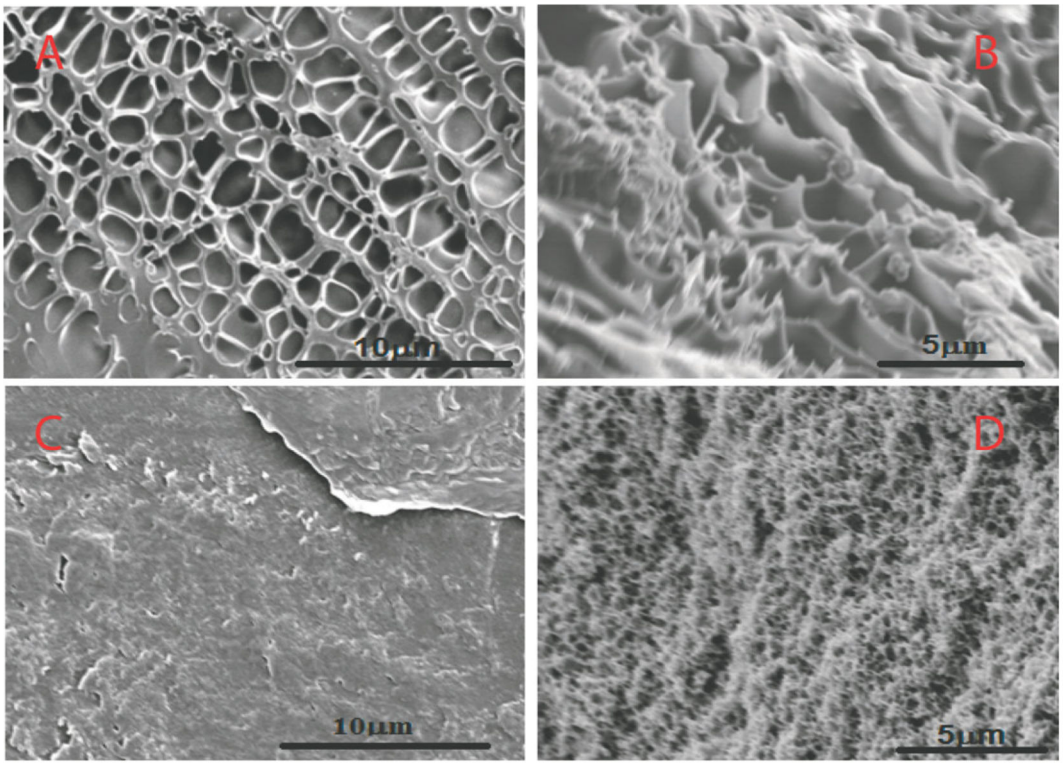

Figure 4.
SEM images of hydrogels after reaching swelling equilibrium at pH 6.5 below LCST at 25°C (A and B: surface and cross-sections, respectively) and above LCST at 40°C (C and D: surface and cross-sections, respectively).

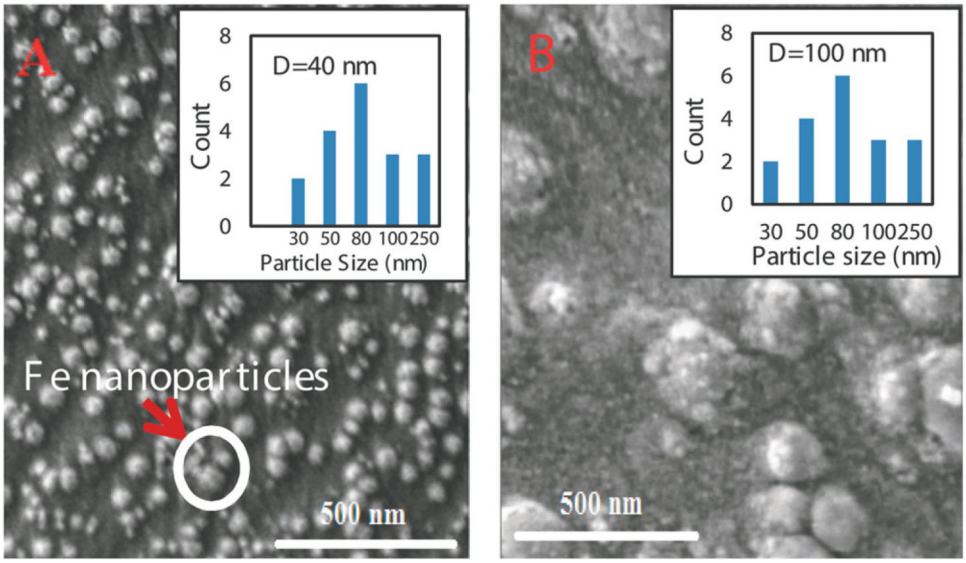

Figure 5.

SEM images of Fe^0 nanoparticles immobilized in P(NIPAAm-AA) hydrogel, A-Fe^0 nanoparticles immobilized in hydrogel by *in situ* synthesis; B-Fe^0 nanoparticles immobilized in hydrogel by encapsulation. [Color figure can be viewed in the online issue, which is available at wileyonlinelibrary.com.]

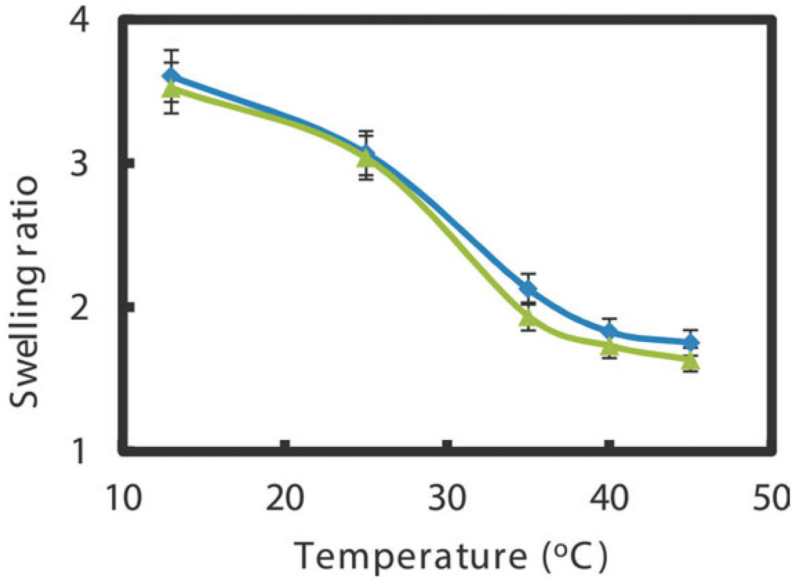

Figure 6.

Swelling ratios of different systems at different temperatures. Diamonds: blank P(NIPAAm-AA) hydrogel without any nanoparticles (blue); triangles: P(NIPAAm-AA) hydrogel with 0.95 wt % nanoparticles by *in situ* synthesis (green) (dry weight: 0.2 g, pH at 25°C: 6.86). [Color figure can be viewed in the online issue, which is available at wileyonlinelibrary.com.]

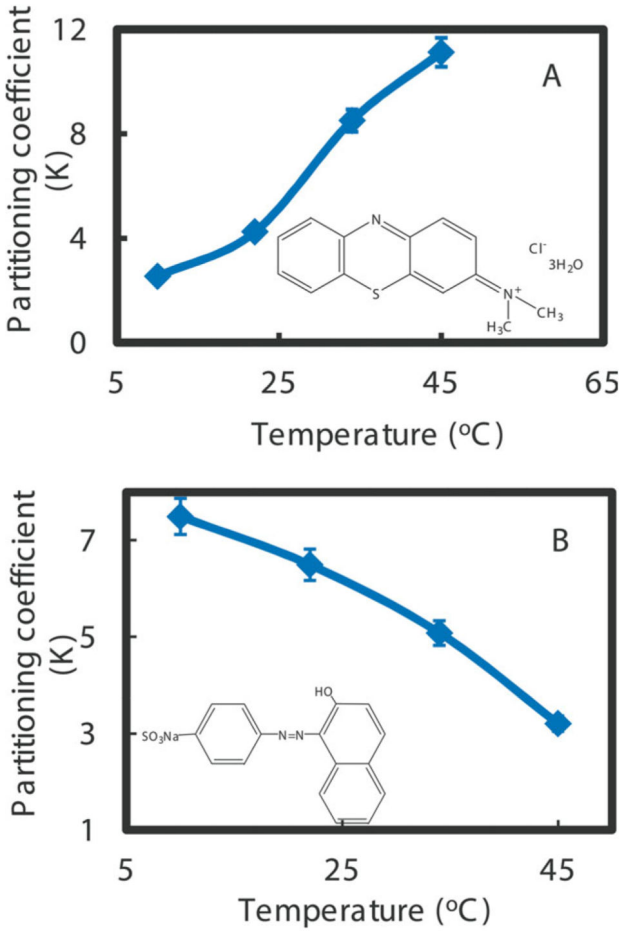

Figure 7.

Partitioning coefficients (*K*) of hydrophobic methylene blue (A) and hydrophilic orange II (B) through P(NIPAAm-AA) hydrogel as a function of temperature (pH = 6.5). The insets are the molecular structures of methylene blue (A) and orange II (B). [Color figure can be viewed in the online issue, which is available at wileyonlinelibrary.com.]

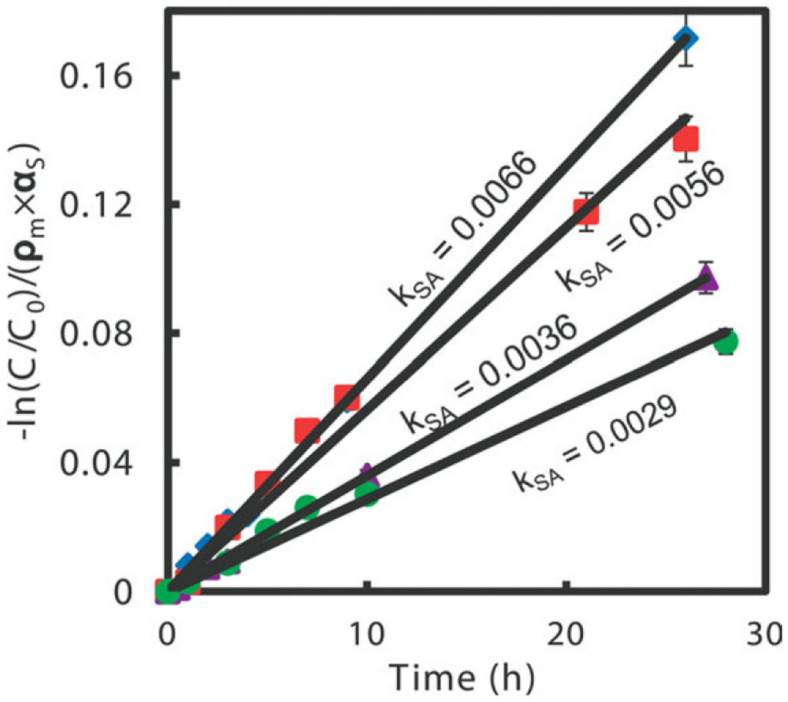

Figure 8.

TCE dechlorination of deionized ultrafiltered water (DIUF) and "real" water (Paducah, KY) with Fe nanoparticles *in situ* and encapsulated in P(NIPAAm-AA) hydrogel (Diamond: Fe (*in situ*) with DIUF water; Square: Fe (*in situ*) with real water; Triangle: Fe (encap.) with DIUF water; Circle: Fe (encap.) with real water). Vol. = 43 mL, initial pH: 7 (for DIUF) and 7.5 (for real water); initial TCE concentration: 30 mg L^{-1}, iron loading amount: 1 g L^{-1}; Temperature: 25°C. [Color figure can be viewed in the online issue, which is available at wileyonlinelibrary.com.]

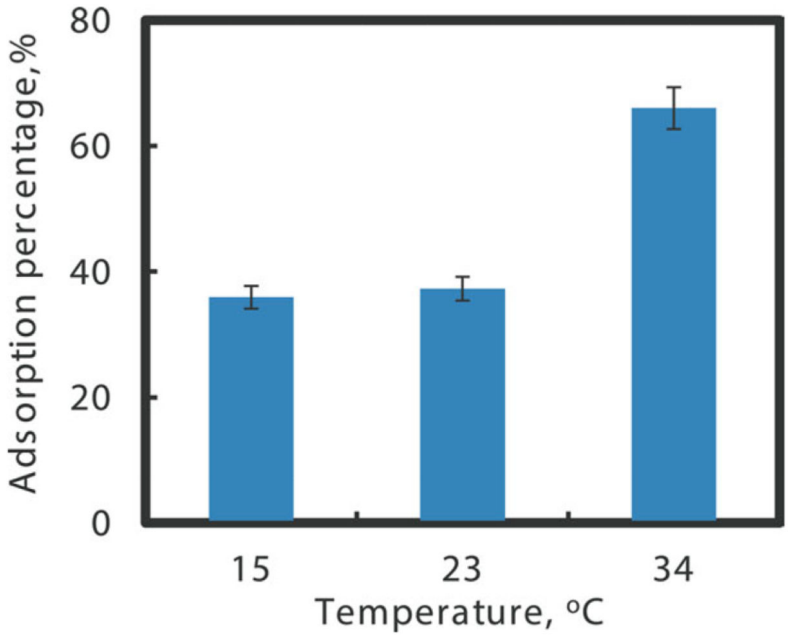

Figure 9.

Normalized TCE adsorption through temperature responsive P(NIPAAm-AA) hydrogel below LCST (15 and 23°C) and above LCST (34°C), feed concentration: 0.2 m*M* TCE, 20 mL, pH = 6.8. [Color figure can be viewed in the online issue, which is available at wileyonlinelibrary.com.]

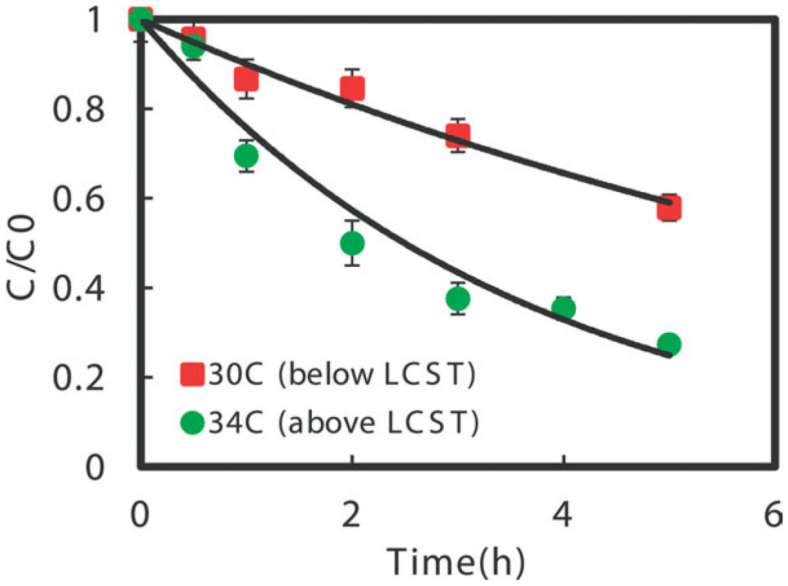

Figure 10.

Batch dechlorination of TCE with Fe/Pd (Pd = 1.5 wt %) (70 nm) immobilized in P(NIPAAm-AA) hydrogel at 30°C (below LCST) and 34°C (above LCST). Vol. = 43 mL, pH = 6.8; initial TCE concentration: 30 mg L^{-1}, iron loading amount: 0.3 g L^{-1}. [Color figure can be viewed in the online issue, which is available at wileyonlinelibrary.com.]

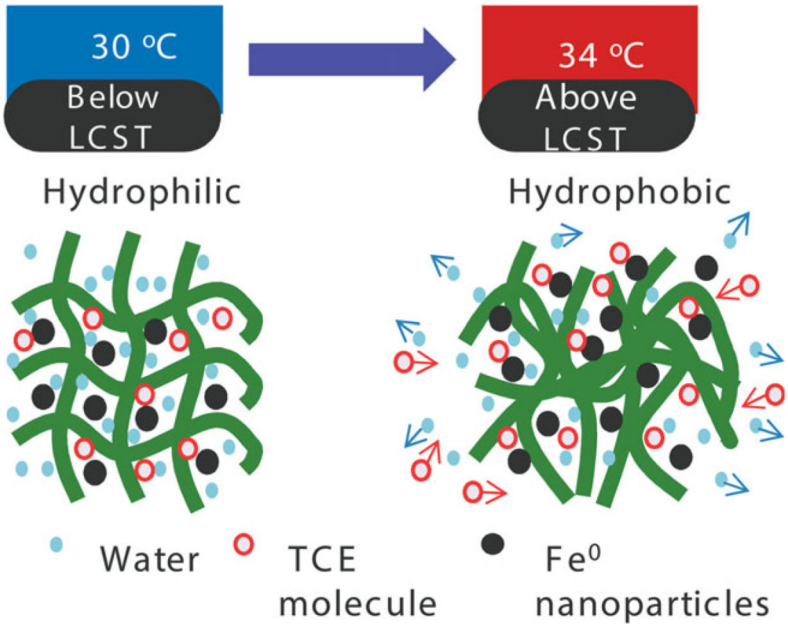

Figure 11.

Schematic of temperature behavior and transport of reagents with temperature responsive hydrogel immobilized Fe^0 nanoparticles. [Color figure can be viewed in the online issue, which is available at wileyonlinelibrary.com.]